

Microstructure Evolution and Corrosion Behavior of Duplex Stainless Steel During Isothermal Aged at 650 °C

Liang He^{1,2}, Xiayu Wu², Ziyang Zhang¹, Jin Li^{2,*}

¹ School of Materials Engineering, Shanghai University of Engineering Science, Shanghai 201620, China

² Department of Materials Science, Fudan University, Shanghai 200433, China

*E-mail: corrosion@fudan.edu.cn

Received: 21 June 2016 / Accepted: 28 July 2016 / Published: 7 August 2016

Duplex stainless steel are used extensively for both strength and corrosion performance, but owing to its complex dual phase structure, there will be a variety of precipitation phases in the procedure of thermal process. In the present paper, the precipitation evolution and corrosion behavior of SAF2205 isothermal aged at 650 °C for various aging times up to 100 h was investigated. The microstructure evolution showed that with the increased of aging time, some chromium-rich intermetallic phase will precipitation and increased yet. The precipitation included intermetallic (σ , R, τ , χ), carbide and nitride (Cr_2N and M_{23}C_6). DL-EPR test show a good relationship between microstructure and selective corrosion resistance. Simultaneously, on the basis of the EIS measurements the charge transfer resistance and interface adsorption time was obtained and both of which are decreased accompany the increasing of the aging time. The selective corrosion is associated with the chromium and molybdenum depleted zones formed around the precipitates during aging.

Keywords: duplex stainless steel, sensitization, precipitates, intergranular corrosion, EIS

1. INTRODUCTION

Duplex stainless steel (DSS), constituted by ferrite(α)-austenite(γ) dual phase microstructure, are suitable for various applications because of their attractive combination of mechanical and corrosion performance [1, 2]. Generally, approximate equal contents of the two phases, balanced distribution of element of the two phases and a secondary-phase free microstructure are important for the good properties [3-6]. However, during the manufacture and application of DSS, the alloy is inevitable to expose at various thermal cycle, then precipitation of detrimental phases, such as intermetallic phases (σ , χ), carbides, nitrides, is unavoidable [7, 8]. The precipitation of intermetallic

phases is usually associated with some key alloying elements depleted, such as chromium, molybdenum, and nitrogen, leading loss of toughness and corrosion resistance [9-13].

Several researchers investigated the corrosion resistance of the steel about the precipitate nose temperature [14, 15] and 475 °C brittle temperature [16, 17]. And some authors have reported that the selective corrosion behavior of DSS is due to the precipitation of intermetallic phases that led to the regional depletion of chromium and/or molybdenum [5, 18]. However, the discussion about precipitation and corrosion properties for DSS isothermal aging at 650 °C is limited.

Double loop electrochemical potentiokinetic reactivation method (DL-EPR) as a fast, non-destructive and accurate intergranular evaluate way, has been successfully utilized to quantify the degree of sensitization by a lot of authors [15, 19]. EIS (Electrochemical impedance spectroscopy) is another useful way to get the information of the intergranular corrosion susceptibility of DSS, and can offer further information about the obtained electrode structure and interface course [20, 21].

In the present paper, an attempt is to research the microstructure evolution and evaluate the selective corrosion behavior of SAF2205 aged at 650 °C for different aging times, up to 100h. Correspondingly, the effects of heat treatments on microstructure and corrosion properties of SAF2205 were studied.

2. EXPERIMENTAL

2.1. Heat treatment and preparation of specimens

The studied alloy was cut from a sheet of commercial standard SAF2205 duplex stainless steel, with the element compositions is listed in Table 1. In order to homogenization, the hot-rolled steel was solution annealed at 1050 °C in argon atmosphere for 2 h, and then quenched in water. Then these specimens isothermal aging at 650 °C for 0 h (solid solution specimens), 0.5h, 2h, 8h, 32h, 100h, respectively, also protected by argon atmosphere, followed by water quench.

Table 1. Chemical composition of the studied SAF2205

Element	Cr	Ni	Mo	N	Mn	C	Si	S	P	Cu
Wt.%	22.46	5.39	3.11	0.18	1.57	0.016	0.43	0.002	0.03	0.25

The specimens waiting for electrochemical test were mounted with epoxy resin, leaving an exposed surface of 1.0 cm² to the electrolyte. The exposed end was wet ground to 1500 grit and polished by diamond pastes down to 1.5µm, rinsed in ethanol and deionized water prior to the experiment.

2.2. Microstructure characterization

The phase constituents and microstructure of the solution and aging specimens were monitored using scan electron microscope (SEM Phillips XL30 FEG). The metallographic of the aging specimens

were revealed by electrolytic etching in a 10 wt. % oxalic acid solution for 10 s with 2V applied voltage at ambient temperature, then etching in 30 wt. % KOH solution at 2V for 10 s. In order to clearly distinguish the secondary phases, the specimen aging at 650 °C for 32h was analyzed using transmission electron microscope (TEM) (Philips CM20) equipped with a GE twin energy dispersive X-ray (EDX) at 200kV.

2.3. Electrochemical measurements

Electrochemical experiment were performed with three-electrode system, the prepared DSS specimen is working electrode, a platinum foil as auxiliary and a saturated calomel electrode (SCE) were used as reference electrode. Princeton equipment (PARSTAT2273) is used in these experiment.

An optimized double loop electrochemical potentiokinetic reaction (DL-EPR) test method (test solution of 2M H₂SO₄+0.5MNaCl+0.01MKSCN at 30±1 °C) was applied to evaluate the degree of intergranular corrosion susceptibility of SAF2205. The specimen was polarized anodically from -0.40V (a little lower than the corrosion potential) to 0.30V (in the passive area) at the scan speed of 1.667mV/s. Then, the scan was reversed at the same rate until original potential. The current was measured throughout the test, the sensitization intensity was evaluated from the I_r/I_a ratio, where I_a is the peak current of the anodic scan and I_r is the peak current in the reversed scan.

The impedance data were collected at the corroding potential over a frequency range between 100 kHz and 10 mHz with the applied AC amplitude of 10 mV. The data was interpreted on the basis of equivalent electrical circuits using ZSimpWin software for fitting the experimental data.

3. RESULT AND DISCUSSION

3.1. Microstructure observation

Fig. 1 shows the SEM morphology of the specimen aging at various times. For the solid solution condition specimens (Fig.1a), both the austenite (light grey) and ferrite (dark grey) are rearranged along the direction of rolling, and no precipitation can be found in α/γ interface and α/α grain boundary, the interface is thin and clear. Though no obvious precipitated phase can be found in the specimens aged for 30min, but the α/γ interfaces become thick and unclear, as shown in Fig.1b. With increased the aging time, precipitation phase is observed along the α/γ interface and α/α grain boundary, and the precipitates and size increased with prolonged the aging time, see Fig.1c-Fig.1e. When the aging time reached 100h, there are a large amount precipitates in ferrite as represented at Fig.1f.

The thermodynamic equilibrium phase of SAF2205 calculated by Thermo-Calc software is presented in Fig.2. According to the phase diagram, for equilibrium condition at 650 °C, the equilibrium phase mainly consists of α , γ , σ and fewer Cr₂N and M₂₃C₆.

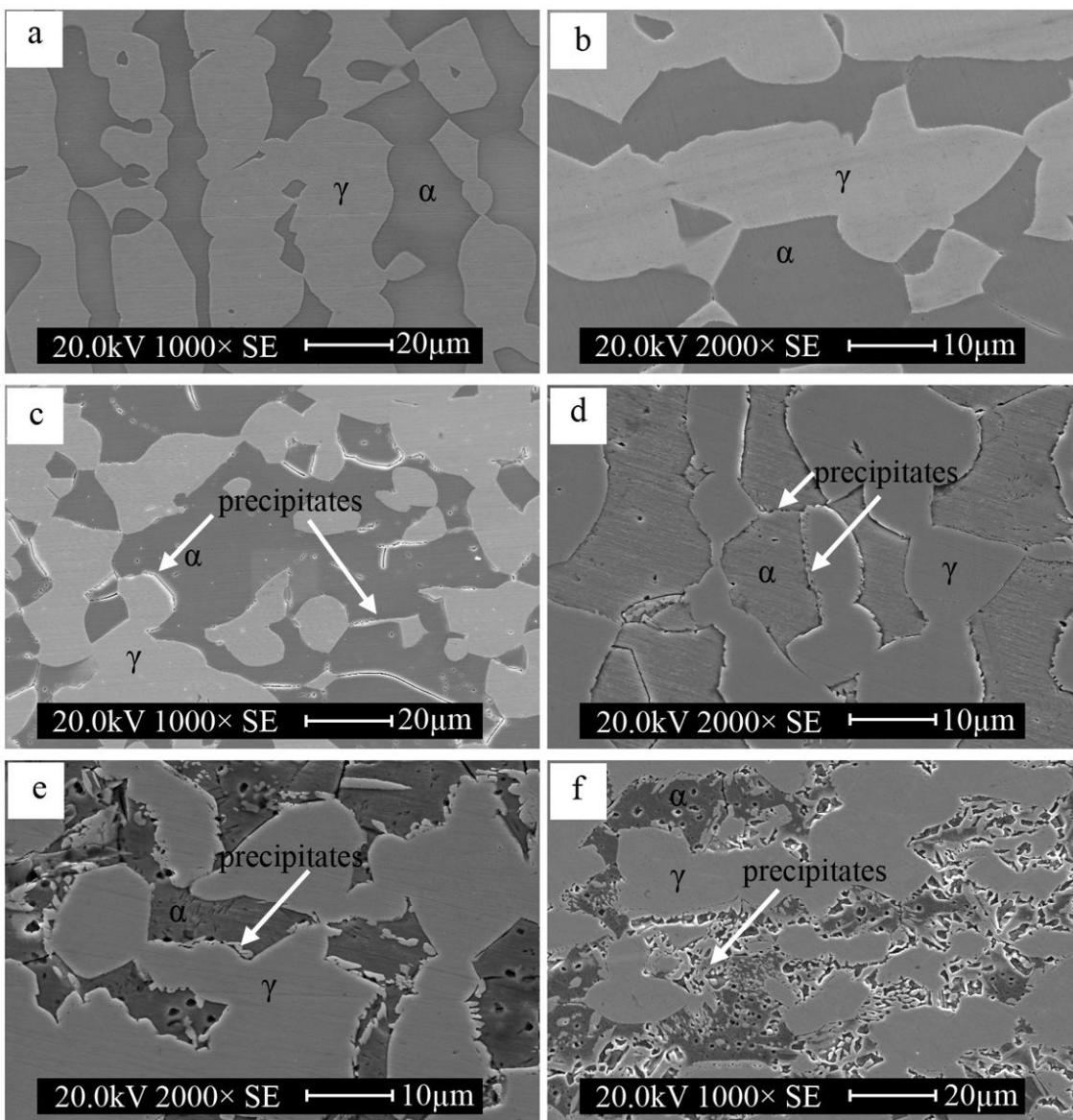


Figure 1. SEM images of SAF2205 aging at 650 °C for various times. a) 0h(as solution annealed) b)0.5h, c)2h, d)8h, e)32h, f)100h.

Because of the technical limitations, SEM, XRD and other technologies are not able to identify the low content phase, in order to better characterize relatively small precipitate phase, TEM is applied to analysis the sample aged at 32h. As shown in Fig.3, intermetallic compound χ and σ main along the α/γ interface and σ with a larger size, R and τ mainly distributed in ferrite phase, R with larger scale and τ shown as flake. As thermodynamic equilibrium phase shown, R, τ , χ were not equilibrium phase, some researcher found prolonged the aging time, χ and R phase will transfer to σ phase[1, 22]. In addition, Cr_2N and M_{23}C_6 with small size can be found in ferrite and at α/γ interfaces. Remarkably, along with the precipitation of these phases, and secondary austenite(γ_2) precipitate synchronously, the generation mechanism main is $\alpha \rightarrow \sigma + \gamma_2$ and $\alpha \rightarrow \text{M}_{23}\text{C}_6 + \gamma_2$. Table 2 show the EDX analysis of the average composition of several important element(wt. %) for the main phases in SAF2205 aged at 650

°C for 32h. As these chromium-rich precipitates, induce chromium-depletion area appeared around the precipitation.

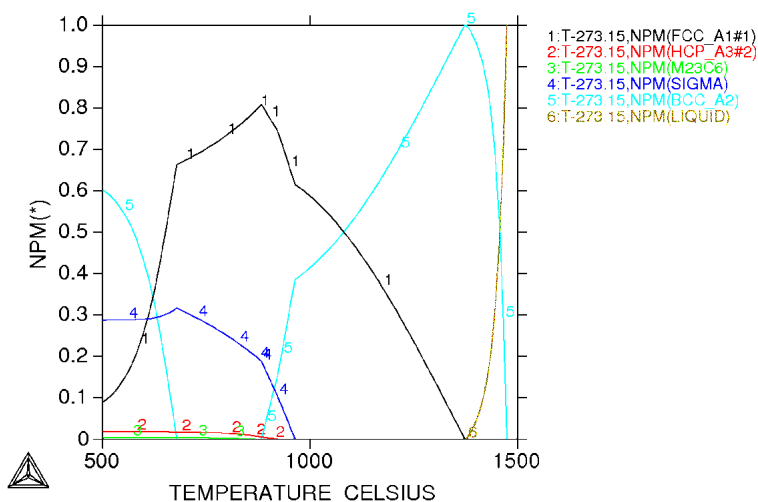


Figure 2. Equilibrium phase fractions in duplex stainless steel 2205 versus temperature by Thermo-Calc software thermodynamic calculation

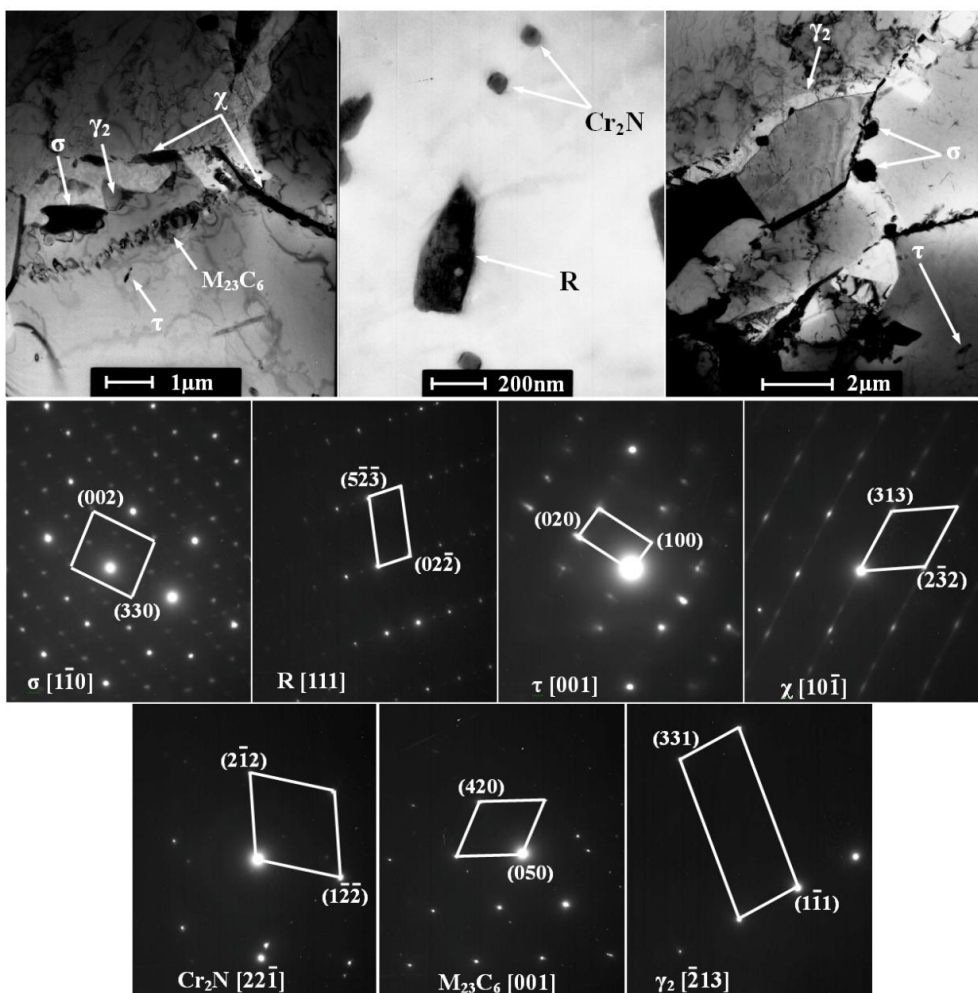


Figure 3. (a) TEM micrographs, (b) Electron diffraction pattern of secondary phases for SAF2205 specimens aged at 650 °C for 32h

Table 2. EDX analysis of the average composition of several important elements (wt. %) for the main phases in SAF2205 aged at 650 °C for 32h

Phase	Fe	Cr	Ni	Mo	Mn
Ferrite (α)	62.8	24.5	2.9	4.9	1.6
Austenite (γ)	65.4	22.1	7.8	3.3	2.1
Secondary Austenite (γ_2)	65.0	17.2	8.1	3.2	2.2
Sigma (σ)	56.7	30.2	2.7	12.5	2.1

3.2. DL-EPR result

The typical DL-EPR curves of SAF2205 aged at 650 °C for different time were shown in Figure 4. All of the DL-EPR curves have obvious passivation area, although some researchers considered that the maximum current density of anodic scanning (I_a) was independent of aging treatment time [23]. But in the present work, I_a value gradually increased with aging time, the I_a of solid solution specimens are $10.98\text{mA}\cdot\text{cm}^{-2}$, but for specimens aged at 650 °C for 100h, the I_a value is up to $59.36\text{mA}\cdot\text{cm}^{-2}$. With the aging time extended, the chromium depleted zone increases, and the corrosion degree of the material is increased, and the corresponding current density will be increased.

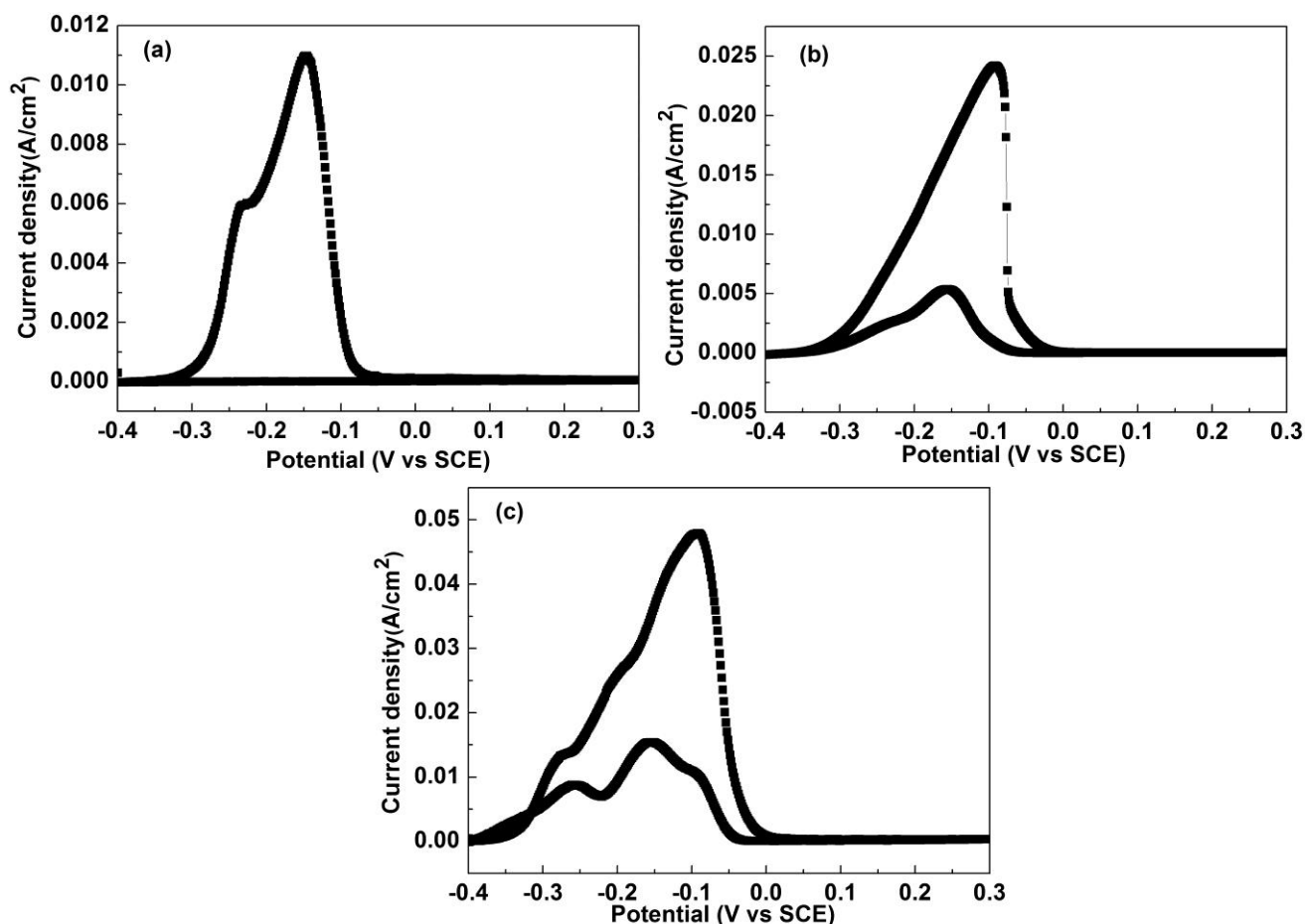


Figure 4. Typical DL-EPR test curves for SAF 2205 isothermal aged for various times (a)0h, (b) 8h,(c)32h. (test solution 2M H_2SO_4 +0.5 M NaCl+0.01 M KSCN, solution temperature 30 ± 1 °C, scan rate 1.667mV/s)

For non-sensitized treatment samples, no current peak (I_r) appears in reverse scan period, as illustrated in Fig.4a, which indicates that under the test conditions, the samples almost does not occur to intergranular corrosion; when the samples were sensitized to 8h, there is a high reverse scan peak I_r (Fig.4b), imply that the sample become sensitive to intergranular corrosion after aging for 8h; the DL-EPR curve has two obvious peaks in Figure 4c. Wu et al. [24] suggested that the positive potential peak corresponds to the intergranular corrosion current and negative potential peak is from the pitting corrosion of the matrix, it mean that the corrosion mechanism evolve from intergranular corrosion to general corrosion.

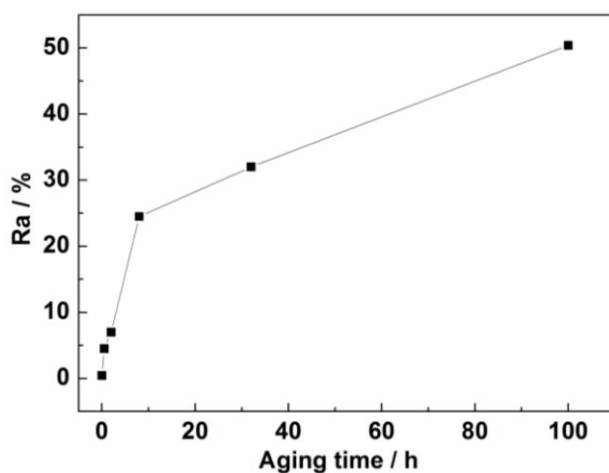


Figure 5. Reactivation rate (Ra) as a function of aging time

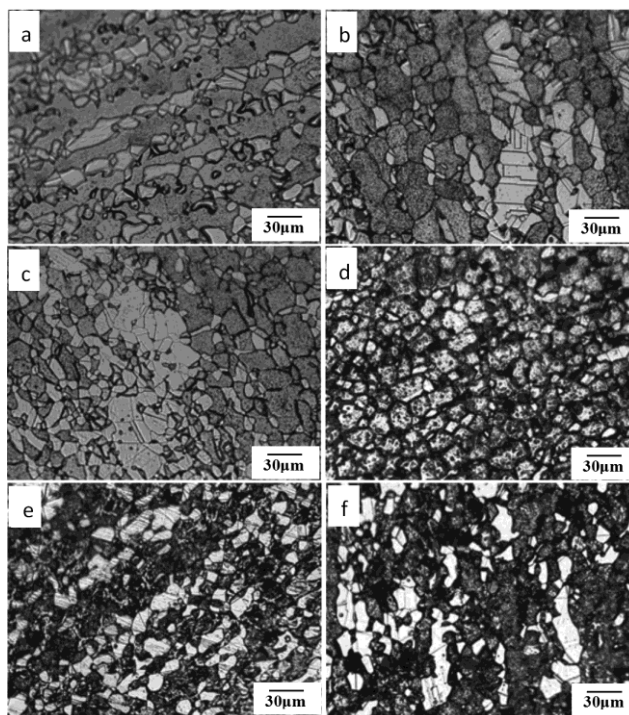


Figure 6. Optical micrographs of SAF2205 aged at 650 °C for various time after DL-EPR test (a)0h, (b)0.5h,(c) 2h,(d)8h,(e)32h,(f)100h

In addition, the maximum current density of anode scanning and cathode reverse scan stage is not in the same voltage, the peak potential of I_a is 30-50mV higher than I_r peaks. This is due to the differential form of ohm impedance. The reactivation rate (R_a) versus aging time is illustrated in Fig.5, it can be found that the R_a increased with prolong of the sensitization time, which indicates that the chromium-depletion area is increased too. The passivation film of the chromium depleted zone is very unstable, so in the scan back stage, easier to be destroyed, leading to very high current of reactivation. This also indirectly shows that with increasing sensitization time, the precipitation of chromium rich phase increased.

Figure 6 shows the microscopic morphology of the samples after DL-EPR test. For solid solution specimens, there is no obvious intergranular corrosion mark, see Figure 6a. After the sensitization of 0.5h, there was obvious intergranular corrosion trace in the ferrite and α/γ phase boundary. When the aging time is prolonged, the intergranular corrosion phenomenon is obvious, see Figure 6 (b) - (e), when the aging time continues to increase to 100h, there is a uniform corrosion phenomenon, the majority of ferrite surface is corroded. As showed in the previous analysis, chromium-rich and chromium-depletion area appeared together, and for a poor chromium phase, due to the relatively low Cr content cannot form a layer of very good protecting chromium oxide film, is likely to decrease the corrosion performance of the zone.

3.3. Electrochemical impedance spectroscopy

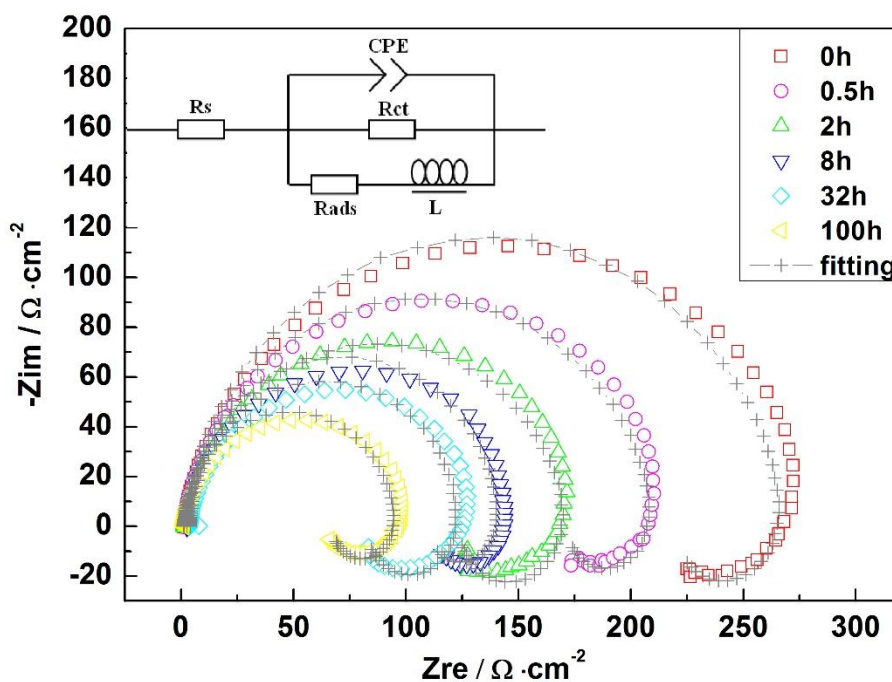


Figure 7. Typical Nyquist curve for SAF2205 aged at 650 °C for various time (test solution 2 M H_2SO_4 +0.5 M NaCl+0.01 M KSCN, 30±1 °C), R_s represents the solution resistance, CPE is for constant phase element, R_{ct} indicates charge transfer resistance, R_{ads} is for adsorption corrosion intermediate impedance, inductance is L

The typical electrochemical impedance spectroscopy of specimens aging at different time is shown in Fig.7a, the equivalent circuit is shown in Fig.7b. As can be seen, the Nyquist diagram of all the specimens with similar shape: at high frequencies is a slightly flattened semicircle, it shows an inductive loop at low frequencies. The capacitive arc radius is related with the charge transfer resistance and the electric double layer on the metal surface [25]. Deviation from perfect semicircle is usually considered as the etching surface rough and uneven. Besides, the surface geometrical feature could affect the current density distribution during the chemical reactions [26,27], which may also influence the corrosion rate.

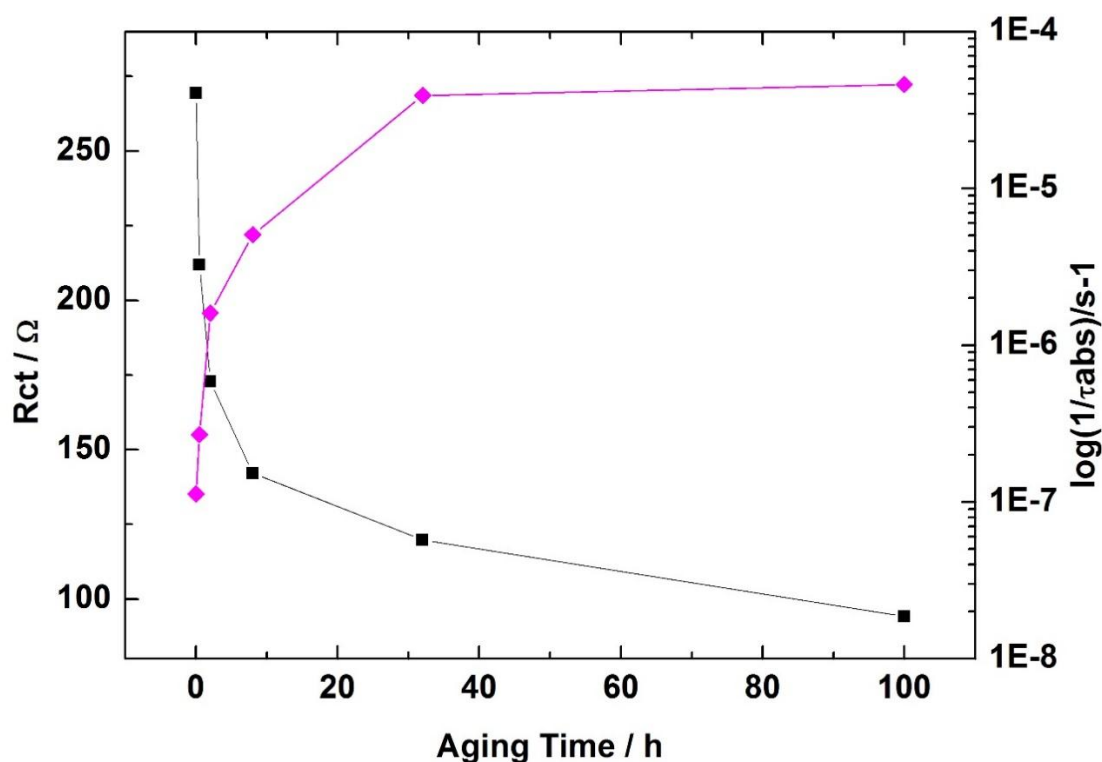
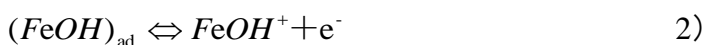


Figure 8. Curve of R_{ct} versus and Intermediate adsorption process versus aging time

The R_{ct} value versus aging time curve is shown in Fig.8. It should be emphasized that R_{ct} contains two parts, namely, the chromium molybdenum depleted region and the rest of the region. In the process of selective corrosion, the resistance of the chromium and molybdenum depletion region is much lower than the rest of the region. Therefore, the R_{ct} value is mainly determined by the resistance of the chromium molybdenum depletion region. As the charge transfer resistance decreases gradually with the aging time, which shows that the area of poor chromium increases gradually with the prolong of the aging time.

Generally, the dissolution of the iron including the following steps:



The first step is ad-atom formation process, $FeFe^*$ and OH^- act as catalyst, the hydroxyl ion stability of a one-valent adsorbed atom of iron, where $(FeOH)_{ad}$ is the most important in the all possible intermediate products [28].

Arutunow reported that the adsorption rate of the intermediate products can be characterized by the $1/(L \cdot R_{ads})$ [20], the adsorption rate of the intermediate products for different aging time is shown on Fig.8 too. Along with the prolong of isothermal aging time, the adsorption rate of the intermediate products increased gradually. These results are consistent with DL-EPR test results.

4. CONCLUSION

(1) SAF 2205 alloy aging treatment at 650 °C, precipitates are mainly R, σ , τ , χ , $M_{23}C_6$ and Cr_2N , meanwhile, a large amount of γ_2 generated. The selective corrosion is mainly caused by precipitates surrounding chromium depleted zone.

(2) Prolong of the aging time, the intergranular corrosion sensitivity of the steel increased, and the corrosion type transfer from intergranular corrosion to uniform corrosion.

(3) Both DL-EPR and EIS can be used to estimate the intergranular corrosion properties of materials, DL-EPR can reflect the degree of intergranular corrosion, EIS result can provide the interface adsorption, charge transfer resistance and other information.

ACKNOWLEDGEMENT

This work is supported by the National Nature Science Foundation of China (Grants No. 51131008, 51501041 and 51371053).

References

1. K.H. Lo, C.H. Shek, J.K.L. Lai, *Mater. Sci. Eng., R*, 65(2009) 39.
2. L. Wickström, K. Mingard, G. Hinds, A. Turnbull, *Corros. Sci.*, 109(2016) 86.
3. J.C. de Lacerda, L.C. Cândido, L.B. Godefroid, *Int. J. Fatigue*, 74(2015) 81.
4. H. Zhao, Z.Y. Zhang, H.Z. Zhang, J. Hu, J. Li, *J. Alloy Compd.*, 672(2016)147.
5. A.R. Akisanya, U. Obi, N.C. Renton, *Mater. Sci. Eng., A*, 535(2012)281..
6. H.S. Choa, K. Lee, *Mater. Charact.*, 75(2013)29.
7. M. Pohl, O. Storz, T. Glogowski, *Mater. Charact.*, 58(2007) 65.
8. Z.Y.Zhang, H.Z. Zhang, H. Zhao, J. Li, *Corros. Sci.*, 103(2016) 189.
9. E. Angelini, B. De Benedetti, F. Rosalbino, *Corros. Sci.*, 46(2004) 1351.
10. S.K. Ghosh, S. Mondal, *Mater. Charact.*, 59(2008) 1776.
11. Y. Li, J. Liu, Y. Deng, X. Han, W. Hu, C. Zhong, *J. Alloy Compd.*, 673 (2016) 28.
12. C. Zhong, F. Liu, Y.T. Wu, J.J. Le, L. Liu, M.F. He, J.C. Zhu, W.B. Hu, *J. Alloy Compd.*, 520 (2012) 11.
13. J.J. Le, L. Liu, F. Liu, Y.D. Deng, C. Zhong, W.B. Hu, *J. Alloy Compd.*, 610 (2014) 173.
14. S.M. Yang, Y.C. Chen, C.H. Chen, W.P. Huang, D.Y. Lin, *J. Alloy Compd.*, 633(2015) 48.
15. N. Ebrahimi, M. Momeni, M.H. Moayed, A. Davoodi, *Corros. Sci.*, 2011. 53(2): p. 637-644.
16. R. Silva, L.F.S. Baroni, M.B.R. Silva, C.R.M. Afonso, S.E. Kuri, C.A.D. Rovere, *Mater. Charact.*, 114(2016) 211.
17. J.D. Tucker, M.K. Miller, G.A. Young, *Acta Metall.*, 87(2015) 15.
18. P.E. Vignal, V. Vignal, S. Saedlou, F. Krajcarz, *Corros. Sci.*, 99(2015) 194.
19. N. Ortiz, F.F. Curiel, V.H. López, A. Ruiz, *Corros. Sci.*, 69(2013) 236.
20. A. Arutunow, K. Darowicki, *Electrochim. Acta*, 54(2009) 1034.

21. A. Arutunow, K. Darowicki, *Electrochim. Acta*, 53(2008) 4387.
22. D.M. Escriba, E. Materna-Morris, R.L. Plaut, A.F. Padilha, *Mater. Charact.*, 60(2009) 1214.
23. J. Gong, Y.M. Jiang, B. Deng, J.L. Xu, J.P. Hu, J. Li, *Electrochim. Acta*, 55(2010) 5077.
24. T. Wu, W. Tsai, *Corros. Sci.*, 45(2003) 267.
25. J. Gao, Y. M. Jiang, B. Deng, W. Zhang, C. Zhong, J. Li, *Electrochim. Acta*, 54(2009) 5830.
26. C. Zhong, X. Tang, Y.F. Cheng, *Electrochim. Acta*, 53 (2008) 4740.
27. J. Liu, W.B. Hu, C. Zhong, Y.F. Cheng, *J. Power Sources*, 223 (2013) 165.
28. W. Plieth, *Electrochemistry for Materials Science*, Elsevier Int., (2008), Amsterdam, Netherlands.

© 2016 The Authors. Published by ESG (www.electrochemsci.org). This article is an open access article distributed under the terms and conditions of the Creative Commons Attribution license (<http://creativecommons.org/licenses/by/4.0/>).